



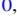




The Open Cluster Chemical Abundances and Mapping Survey. II. Precision Cluster Abundances for APOGEE Using SDSS DR14

John Donor¹, Peter M. Frinchaboy¹ , Katia Cunha², Benjamin Thompson^{1,3}, Julia O’Connell¹ , Gail Zasowski⁴ ,
Kelly M. Jackson^{1,13}, Brianne Meyer McGrath^{1,5}, Andrés Almeida⁶, Dmitry Bizyaev^{7,8}, Ricardo Carrera⁹ ,
D. A. García-Hernández^{10,11}, Christian Nitschelm¹², Kaike Pan⁷ , and Olga Zamora^{10,11}

¹ Department of Physics & Astronomy, Texas Christian University, TCU Box 298840, Fort Worth, TX 76129, USA; j.donor@tcu.edu, p.frinchaboy@tcu.edu,
b.a.thompson1@tcu.edu, j.oconnell@tcu.edu, b.r.meyer@tcu.edu

² Observatório Nacional, São Cristóvão, Rio de Janeiro, Brazil

³ GitHub, Inc., 88 Colin P. Kelly Street, San Francisco, CA 94107, USA

⁴ Department of Physics & Astronomy, University of Utah, 115 S. 1400 E., Salt Lake City, UT 84112, USA

⁵ Department of Physics, University of Colorado Colorado Springs, 1420 Austin Bluffs Pkwy, Colorado Springs, CO 80918, USA

⁶ Instituto de Investigación Multidisciplinario en Ciencia y Tecnología, Universidad de La Serena, Benavente 980, La Serena, Chile; aalmeida@userena.cl

⁷ Apache Point Observatory and New Mexico State University, P.O. Box 59, sunspot, NM 88349-0059, USA; kpan@apo.nmsu.edu, dmbiz@apo.nmsu.edu

⁸ Sternberg Astronomical Institute, Moscow State University, Moscow, Russia

⁹ Astronomical Observatory of Padova, National Institute of Astrophysics, Vicolo Osservatorio 5, I-35122, Padova, Italy; ricardo.carrera@oapd.inaf.it

¹⁰ Instituto de Astrofísica de Canarias, E-38205 La Laguna, Tenerife, Spain; ozamora@iac.es, agarcia@iac.es

¹¹ Universidad de La Laguna (ULL), Departamento de Astrofísica, E-38206 La Laguna, Tenerife, Spain

¹² Unidad de Astronomía, Universidad de Antofagasta, Avenida Angamos 601, Antofagasta 1270300, Chile; christian.nitschelm@uantof.cl

Received 2018 May 2; revised 2018 July 19; accepted 2018 July 24; published 2018 September 6

Abstract

The Open Cluster Chemical Abundances and Mapping (OCCAM) survey aims to produce a comprehensive, uniform, infrared-based spectroscopic data set for hundreds of open clusters, and to constrain key Galactic dynamical and chemical parameters from this sample. This second contribution from the OCCAM survey presents analysis of 259 member stars with [Fe/H] determinations in 19 open clusters, using Sloan Digital Sky Survey Data Release 14 (SDSS/DR14) data from the Apache Point Observatory Galactic Evolution Experiment and ESA *Gaia*. This analysis, which includes clusters with R_{GC} ranging from 7 to 13 kpc, measures an [Fe/H] gradient of -0.061 ± 0.004 dex kpc^{-1} . We also confirm evidence of a significant positive gradient in the α -elements ([O/Fe], [Mg/Fe], and [Si/Fe]) and present evidence for a significant negative gradient in iron-peak elements ([Mn/Fe] and [Ni/Fe]).

Key words: Galaxy: abundances – Galaxy: disk – Galaxy: evolution – open clusters and associations: general

Supporting material: figure set, machine-readable tables

1. Introduction

The detailed chemical evolution of stars in galaxies provides key information on how galaxies grow and evolve. Star clusters provide an age-datable tracer for measuring the growth and evolution of the Galaxy. One key measurement is the disk radial chemical trend or gradient as traced by open clusters (Janes 1979). The Galactic abundance gradient has been fit by a single linear gradient (e.g., Friel & Janes 1993; Friel 1995; Carraro et al. 1998; Friel et al. 2002), and increasingly more commonly by a 2-function gradient (e.g., Bragaglia et al. 2008; Sestito et al. 2008; Friel et al. 2010; Carrera & Pancino 2011; Reddy et al. 2016).

Recent work using open clusters has consistently found a metallicity gradient ($d[\text{Fe}/\text{H}]/dR_{GC}$) between roughly -0.05 dex kpc^{-1} (Reddy et al. 2016, hereafter R16) and -0.09 dex kpc^{-1} (Friel 1995; Carraro et al. 1998; Yong et al. 2012) for clusters between $6 \text{ kpc} < R_{GC} < 14 \text{ kpc}$. Others have reported qualitatively similar trends, but do not quote a metallicity gradient measurement (Donati et al. 2015; Magrini et al. 2015, 2017; Casamiquela et al. 2017). But while the general negative shape of the abundance trend is well agreed upon, no consensus has been reached on the steepness of the gradient. Carrera & Pancino (2011) shed some light on this discrepancy by showing the difference between a gradient

measured to $R_{GC} = 12.5 \text{ kpc}$ (-0.070 ± 0.005) all the way to $R_{GC} = 25 \text{ kpc}$ (-0.046 ± 0.010); Frinchaboy et al. (2013) show a similar discrepancy using [M/H].

Another unavoidable problem that has made this measurement difficult is systematic offsets between studies of chemical abundance and distance. This inevitably introduces some systematic uncertainties when a compilation of results from the literature is used. Recent work has sought to correct for systematic uncertainties by “homogenizing” their samples. R16 take equivalent width measurements from the literature but use a uniform line list for their analysis. Netopil et al. (2016) homogenized a large photometric sample using a literature compilation of high-resolution spectroscopic studies; however, they do not homogenize the spectroscopic studies.

This paper presents an important contribution to the field by utilizing a homogeneous spectroscopic data set, with all stars observed by the same telescope and analyzed with the same abundance analysis pipeline: the Apache Point Observatory Galactic Evolution Experiment (APOGEE; Majewski et al. 2017). We present a high-reliability sample of stars that are open cluster members, bulk cluster parameters, and Galactic abundance gradient using the APOGEE/Open Cluster Chemical Abundances and Mapping (OCCAM) DR14 sample. This paper is organized as follows: The OCCAM target selection is presented in Section 2 and cluster membership analysis in Section 3. We compare our work to other studies in Section 4.

¹³ Current Address: Texas Instrument Corporation, Fort Worth, TX.

Finally, in Section 5 we present our findings on the Galactic metallicity gradients using APOGEE-based abundances, and in Section 6 we consider gradients in other elements.

2. OCCAM Target Selection

The OCCAM target selection includes targets selected in two different ways. First, we selected known members of a subset of open clusters that were observed for calibration purposes. Stars with previous abundance determinations (e.g., Cohen 1980; Smith & Suntzeff 1987; Tautvaišienė et al. 2000; Bragaglia et al. 2001; Yong et al. 2005; Carraro et al. 2006; Carretta et al. 2007; Origlia et al. 2006; Pancino et al. 2010; Basu et al. 2011) and/or high-quality RV-based membership studies (e.g., Geller et al. 2008, 2010; Mermilliod et al. 2008; Hole et al. 2009) were targeted. These calibration cluster targets can be identified in DR14 through a specific targeting flag (*apogee_target2* = 10 and/or *apogee2_target2* = 10; Zasowski et al. 2013, 2017).

The second method selected “likely” cluster targets based upon their location in the cluster color–magnitude diagram (CMD) using the colors in the surveys 2MASS (Cutri et al. 2003) and *WISE* (Wright et al. 2010).

The combination of 2MASS and *WISE* photometry allows for a direct assessment of the line-of-sight reddening to any particular star. The long wavelength regime of spectral energy distributions (SEDs) of stars have the same Rayleigh–Jeans shape, equivalent to saying that the Vega-based, *intrinsic* colors of all stars are nearly constant for the correct combination of filters, as seen in Figure 5 of Majewski et al. (2011). Thus, the *observed* mid-IR colors contain information on the reddening of a star *explicitly*, whereas the NIR SEDs contain information on the stellar types.

By assuming constancy of the intrinsic stellar ($H-4.5\ \mu\text{m}$) colors in the Rayleigh–Jeans regime, $E(H-4.5\ \mu\text{m})$ is derived directly from the observed ($H-4.5\ \mu\text{m}$) color (Majewski et al. 2011). The spread from different populations, RGB, red clump and main sequence, is minimized for this combination, yielding an intrinsic spread of less than 0.09 mag in color for all but the reddest and bluest stars. Since the primary purpose in using this technique is to “clean” the cluster from the field, small systematics are not a concern. Also, the reddest main-sequence stars that would belong to a cluster are too faint for these surveys.

Frinchaboy et al. (2010) devised a technique to utilize the extinction (A_{K_s}) derived from the RJCE technique to distinguish and isolate cluster stars from foreground and background contamination. This technique consists of isolating a region of approximately twice the cluster’s catalog radius (R_{Dias} ; Dias et al. 2002) and dividing it into five regions (see Figure 1(a)). We utilize four “field” regions and the cluster region (radius = R_{Dias}). The field is divided in order to account for dust clouds and any other source of background variability.

We subtract the median area-scaled “field” star density from the “cluster” star numbers within a given A_{K_s} range, and scan this range across all available A_{K_s} values that have at least 15 stars (see Figure 1(b)). The window of extinction with the highest concentration of stars within the inner radius will reveal the cluster (Figures 1(c) and (d)). We then optimize the cluster isolation surveying a grid of A_{K_s} width, A_{K_s} stepsize, and allowed $\sigma_{A_{K_s}}$ values.

We present a demonstration of this technique utilizing the cluster King 7, shown in Figure 1. Figure 1(a) first shows the area explored by our analysis in Galactic latitude and longitude.

As described above, we selected likely cluster members utilizing the A_{K_s} as shown in Figure 1(b). For King 7, we find a low, but nonnegligible extinction or reddening to the cluster. A CMD of this cluster (Figure 1(c)) is generated that highlights the member stars with A_{K_s} values within the selected window of extinction, where the dashed box denotes the area where the SDSS/APOGEE project selects targets ($8.0 < H < 12.2$ and $J - K_s \geq 0.5$). Finally, we compare our “cleaned” cluster CMD to the Padova isochrone (Bressan et al. 2012) utilizing catalog values (Dias et al. 2002) for King 7 and find a good match. By comparing the CMD with isochrone values, when available, we are able to isolate candidate open cluster stars with a high probability for membership. The APOGEE project requires this cleaning for most clusters for three reasons: (1) most open clusters are found at low Galactic latitude and thereby are heavily contaminated with field stars. (2) Due to the large SDSS telescope field of view (Gunn et al. 2006), the minimum fiber-to-fiber distance is fairly large (≥ 1 arcmin), which only allows for the targeting of a handful of stars ($\sim 5-10$) per cluster for the most poorly studied, distant, and reddened clusters. (3) Prior to *Gaia*, the proper motion data required for high-quality reliable membership determinations were only available for a few clusters.

Likely open cluster members selected by this method are identified in DR14 (Abolfathi et al. 2018), and previous DRs (10,12,13) through specific targeting flag (*apogee_target1* = 9 and/or *apogee2_target1* = 9; Zasowski et al. 2013, 2017).¹⁴

3. Analysis

3.1. OCCAM Observed Stars in SDSS4 DR14

The primary spectroscopic data for OCCAM comes from the APOGEE (Majewski et al. 2017), which is part of the Sloan Digital Sky Survey-III and IV surveys (SDSS; Eisenstein et al. 2011; Blanton et al. 2017), utilizing the 2.5 m Sloan Foundation telescope (Gunn et al. 2006) at Apache Point Observatory. APOGEE is a near-infrared (1.514–1.696 μm) spectroscopic survey, primarily focusing on the Galactic disk (Zasowski et al. 2013, 2017). The survey uses multi-fiber spectrographs (Wilson et al. 2012), allowing for simultaneous observations of 300 stars.

The APOGEE data reduction pipeline (Holtzman et al. 2015; Nidever et al. 2015) provides high-precision radial velocities (RVs). Stellar parameters (T_{eff} , $\log g$, [M/H], [C/M], [N/M], [α /M]), and detailed abundances for individual elements, such as, Fe, C, N, O, Al, Si, Ca, Ni, Na, S, Ti, Mn, K, and Cu, are derived automatically by the ASPCAP pipeline (García Pérez et al. 2016). The APOGEE survey provides the *uniform* chemical data that underpin this study of open cluster members.

The targets selected for analysis were observed from 2011 August to 2014 July (APOGEE-1), and from 2014 July to 2016 July (APOGEE-2). These data were released as part of the 14th Data Release of SDSS (DR14; Abolfathi et al. 2018), which included APOGEE data for over 250,000 stars. All APOGEE data, from the beginning of APOGEE-1, were reduced using the latest data reduction pipeline (full description of this pipeline is presented in Holtzman et al. 2018).

¹⁴ We did not limit our analysis to stars with just these targeting flags. Random field stars and additional specific targeted cluster programs, and other calibration flags may also apply to the targets analyzed here.

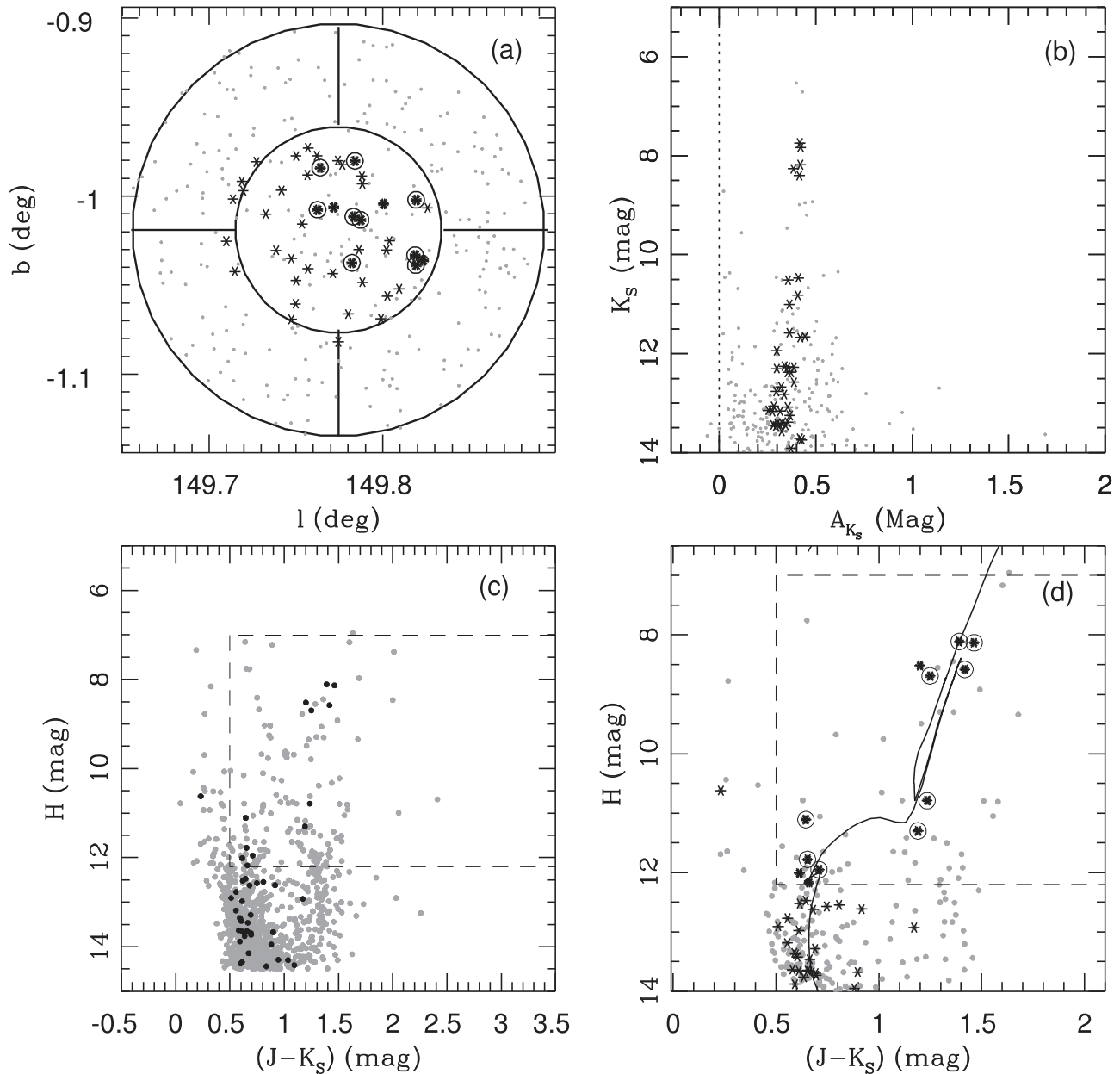


Figure 1. Sample analysis for the cluster King 7 utilizing 2MASS+WISE data (Frinchaboy et al. 2010). (a) Galactic latitude and longitude for all stars (gray) within the $2R_{cl}$ area to be analyzed, stars selected to be likely members from the photometry extinction analysis are shown in black. Prime APOGEE targets are circled. (b) Distribution of A_{K_s} for all stars in the NGC 6802 sample area, black points denote stars with $1.1R_{cl}$ within the determined mean cluster A_{K_s} range. (c) Color-magnitude diagram (CMD) for all stars in the analysis area (gray). The dashed box denotes the SDSS-III/APOGEE target selection region. Black points denote stars selected as likely members from their A_{K_s} . (d) CMD of only likely cluster members overplotted with the Padova Isochrone (Marigo et al. 2008) using the clusters parameters from Dias et al. (2002). Circled stars denote identified high-probability stars for APOGEE target selection (also see the sky distribution (a)).

For this study, we analyzed all stars within $2 \times$ the cluster radius (Kharchenko et al. 2013) for 19 clusters that resulted in a sample of 1361 stars. This entire sample is listed in Table 1 for reference, along with our final membership probabilities and a classification for each star (Section 3.2).

3.2. OCCAM Membership Criteria

Using the stellar radial velocities and derived metallicities as initial discriminators, APOGEE data alone can provide a first guess at cluster membership based on the “bulk” RV and $[\text{Fe}/\text{H}]$ for the cluster region on the sky and comparing each star to the average values. We then further constrain the

membership using proper motions measured by *Gaia* (Gaia Collaboration et al. 2016, 2018; Lindegren et al. 2018).

3.2.1. Quantifying Membership Probability

The “bulk” behavior is found by convolving all measurements using a Gaussian kernel smoothing routine, based on the methods from Frinchaboy & Majewski (2008). The first analysis is in RV. In order to distinguish the cluster from field stars, two samples are computed: stars within two cluster radii (from Kharchenko et al. 2013, except where we enforced a minimum radius of 5 arcmin) of the cluster center, and stars between one and two cluster radii of the center. The results from the “outer” stars are subtracted from the “total” result,

Table 1
OCCAM Sample from APOGEE Data Used for Membership Analysis

Cluster name	2MASS ID	RV (km s ⁻¹)	[Fe/H] (dex)	μ_{α}^a (mas yr ⁻¹)	μ_{δ}^a (mas yr ⁻¹)	RV Prob	[Fe/H] ^b Prob	PM Prob	Member ^c
NGC 6819	2M19401402+4016306	-56.4 ± 0.0	+0.06 ± 0.01	-5.85 ± 0.03	-9.04 ± 0.03	0.00	0.00	0.00	NM
NGC 6819	2M19401466+4004598	-18.9 ± 0.0	-0.03 ± 0.01	+50.96 ± 0.04	+99.82 ± 0.04	0.00	-1.00	0.00	NM
NGC 6819	2M19401937+4015495	-52.3 ± 0.2	-0.35 ± 0.01	-5.93 ± 0.03	-6.26 ± 0.03	0.00	0.00	0.00	NM
NGC 6819	2M19402284+4006008	-50.3 ± 0.1	-0.34 ± 0.01	-1.60 ± 0.03	-2.91 ± 0.03	0.00	0.00	0.00	NM
NGC 6819	2M19403569+4005038	+2.7 ± 0.1	-0.45 ± 0.01	-3.76 ± 0.03	-3.46 ± 0.03	0.00	0.00	0.00	NM
NGC 6819	2M19403684+4015172	+2.1 ± 0.0	+0.15 ± 0.01	-3.00 ± 0.03	-3.66 ± 0.03	0.00	0.00	0.54	NM
NGC 6819	2M19404262+4003043	-35.2 ± 0.1	+0.07 ± 0.01	-4.36 ± 0.04	-19.13 ± 0.04	0.00	0.00	0.00	NM
NGC 6819	2M19404341+4020235	-11.8 ± 16.3	-0.01 ± 0.01	+0.65 ± 0.09	-3.89 ± 0.09	0.00	-1.00	0.00	NM
NGC 6819	2M19404803+4008085	+2.4 ± 0.1	+0.09 ± 0.01	-2.98 ± 0.04	-3.83 ± 0.04	1.00	0.82	0.94	GM
NGC 6819	2M19404965+4014313	+3.1 ± 0.0	+0.12 ± 0.01	-2.84 ± 0.03	-3.72 ± 0.03	0.96	0.94	0.70	GM
NGC 6819	2M19405020+4013109	+4.3 ± 0.0	+0.15 ± 0.01	-3.03 ± 0.04	-3.84 ± 0.04	0.67	0.59	0.85	GM

Notes.

^a From *Gaia* DR2 (Gaia Collaboration et al. 2018; Lindegren et al. 2018)

^b A [Fe/H] membership probability of -1 corresponds to a check against log(*g*) for [Fe/H] reliability. Stars that failed may be members but are flagged because [Fe/H] is not a reliable membership discriminator for these stars.

^c Possibilities here are: GM (giant member), DM (dwarf member), and NM (non-member). We differentiate between giants and dwarfs due the log(*g*) cut mentioned previously: these dwarfs may be members, but their metallicities may not be reliable.

(This table is available in its entirety in machine-readable form.)

leaving a peak where the cluster stars fall, as seen in Figure 2(e) (in blue).

The process is repeated for [Fe/H], seen in Figure 2(f) (in blue) this time subtracting the stars farther than 3σ from the cluster RV previously identified from the whole field (σ is small in practice; thus, 3σ is appropriate for keeping cluster stars without including field stars incidentally close in RV space). If there are at least two APOGEE stars that are cluster members, the smoothing routine will leave behind a larger peak where their values combined. The shape is approximately Gaussian, so a Gaussian profile is fit for both RV and [Fe/H]. When normalized, this Gaussian fit can be used as a membership probability distribution in RV or [Fe/H] space, seen in Figures 2(e) and (f) (overlaid in orange).

Using proper motion data from *Gaia* DR2 (Gaia Collaboration et al. 2016, 2018; Lindegren et al. 2018), a two-dimensional (2D) Gaussian smoothing routine is applied in proper motion space. Again, two samples are computed: all stars within twice the cluster radius and stars outside the cluster’s radius, then the outside sample is subtracted from the full sample. A 2D Gaussian is fit to the remaining peak and membership probabilities are assigned, shown in Figure 2(d).

Finally, a 3σ criterion is adopted for likely membership: a star with parameters falling within 3σ of the cluster mean in [Fe/H], RV, and proper motion is considered a likely member of the cluster. Due to diffusion effects that are present in the abundances of main-sequence and turn-off stars (Souto et al. 2018), and the lack of calibrated DR14 abundances for dwarfs observed in the APOGEE survey (Abolfathi et al. 2018; Holtzman et al. 2018), we restricted our final sample to stars having $\log(g) \lesssim 3.7$. Stars passing an RV and proper motion membership cut but falling above the $\log(g) \approx 3.7$ cut are identified as dwarf members (“DM”),¹⁵ while those falling below the $\log(g)$ cut are identified as giant members (“GM”). Only the giant members are included in the final OCCAM

sample. All stars not falling into either the DM or GM category are identified as non-members (“NM”). Table 1 shows the sample of stars used, with the relevant stellar parameters used and final membership determinations.

The 19 clusters studied in this work were chosen because they had at least four member *giant* stars.

3.2.2. Verifying Membership

Figure 2(a) shows the CMD for NGC 7789, with identified APOGEE members shown in orange and non-members in blue; 2(c) shows the cluster area on the sky for reference. While some members may have been falsely rejected, obvious non-members are clearly rejected. The $T_{\text{eff}}-\log(g)$ diagram in Figure 2(b) shows likely members where they are expected. Figure 2(d) shows a proper motion contour plot, from the 2D Gaussian fit discussed above, which shows members where they are expected. Figure 2(d) also shows some proper motion members rejected for RV and/or metallicity.

All APOGEE cluster and star data, including membership probabilities and abundances plus bulk cluster properties, has been released as part of an SDSS DR14 mini-data release scheduled for the end of 2018 July. The catalog is available at: http://www.sdss.org/dr14/data_access/value-added-catalogs/.

3.3. Measured Cluster Bulk Abundances

A “high-reliability” criterion is adopted for a cluster to be included in our sample: four or more likely member stars, as determined above. This resulted in a total sample of 259 member stars in 19 clusters used for the analysis of galactic abundance gradients.

The final value for [Fe/H] used for computing metallicity gradients is taken to be the mean metallicity of the likely members. The uncertainty on this value is taken to be the standard deviation of the mean metallicity for the cluster. We note that the uncertainties in the metallicities for the individual stars as reported in DR14 are typically ~ 0.01 dex, which may be an underestimation. We therefore disregard these uncertainties in our consideration of the uncertainty in the cluster metallicity.

¹⁵ We note the existence of a few stars with missing calibrated log(*g*) values that consequently fail our log(*g*) cut, even though they are likely giant members, which result in a “dwarf member” (DM) classification.

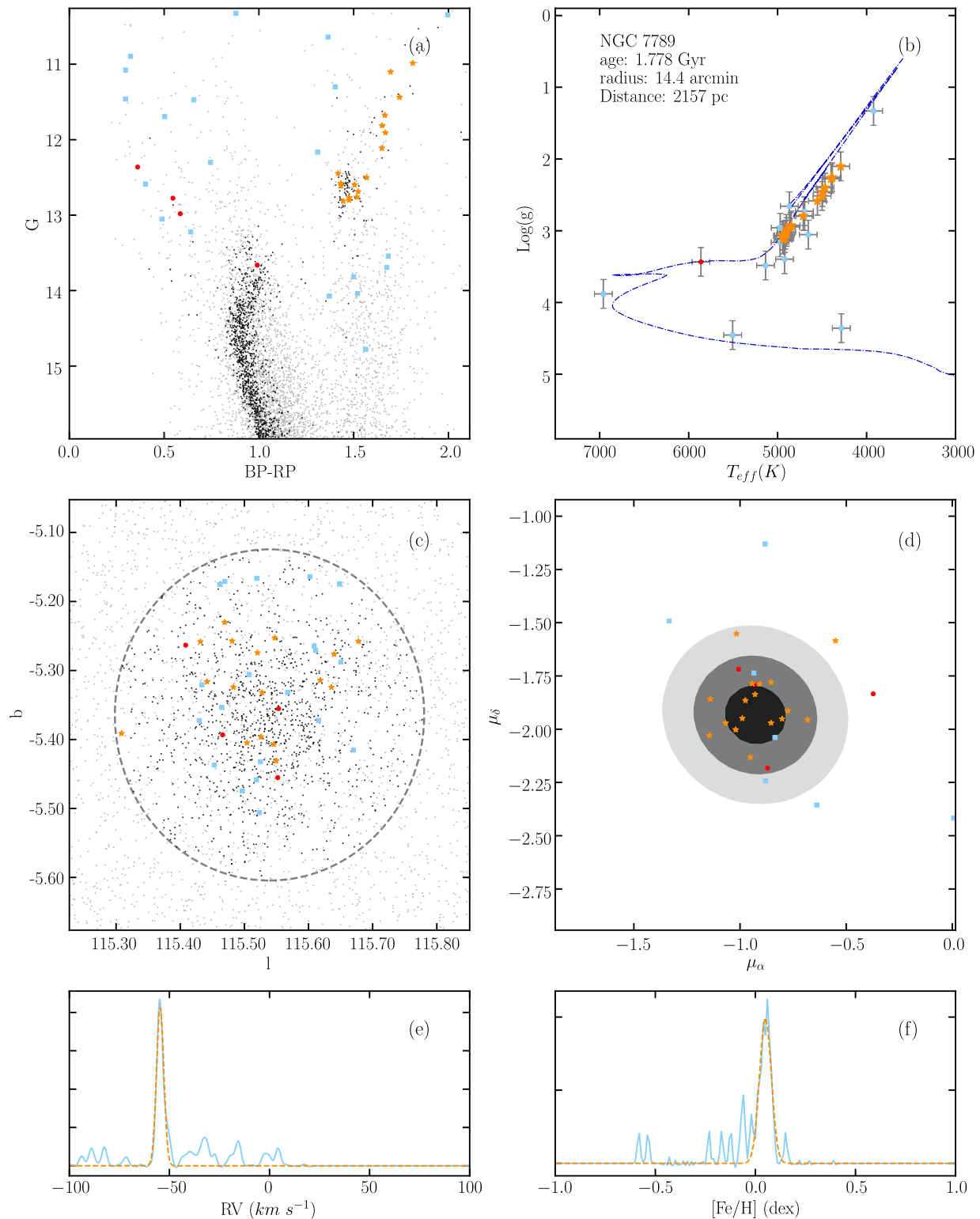


Figure 2. A summary of the membership analysis for open cluster NGC 7789. The complete figure set (19 images) is available in the online journal. (a) The *Gaia* CMD (Gaia Collaboration et al. 2018; Riello et al. 2018), with proper motion members shown in black, others in gray. Likely APOGEE members are shown as orange stars, non-members as blue squares, and APOGEE stars passing an RV and proper motion membership cut, but failing a $\log(g)$ cut for metallicity reliability are shown as red circles. (b) The $T_{\text{eff}}-\log(g)$ diagram for the cluster with an isochrone based on MWSC Catalog ages (Kharchenko et al. 2013) shown for reference. Error bars shown are characteristic, and a possible global offset in $\log(g)$ is seen. (c) The cluster area on the sky. (d) A contour plot of the 2D Gaussian fit to the kernel smoothed proper motions. Contours show 1σ intervals. (e) The Gaussian kernel density convolution in RV , with a Gaussian fit shown in orange. (f) The Gaussian kernel density convolution in $[\text{Fe}/\text{H}]$, with a Gaussian fit shown in orange.

(The complete figure set (19 images) is available.)

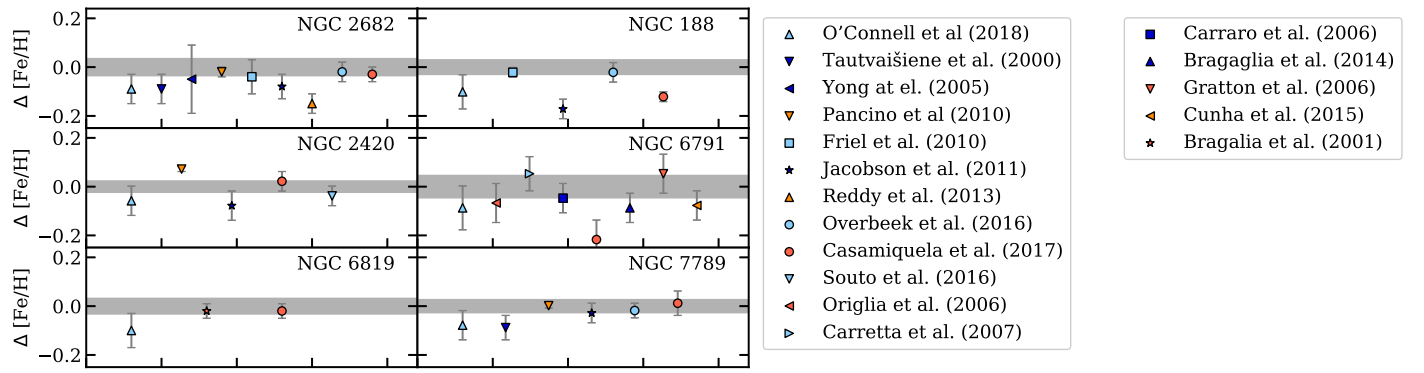


Figure 3. A comparison to commonly studied clusters in the literature ($\Delta[\text{Fe}/\text{H}] = \text{literature} - \text{OCCAM}$). The gray bar indicates the internal 1σ standard deviation for stars in each cluster from our data.

Table 2
OCCAM Data Sample

Cluster Name	l (deg)	b (deg)	Radius ^a (′)	Age ^a (Gyr)	R_{GC} ^b (kpc)	μ_{α} ^c (mas yr ⁻¹)	μ_{δ} ^c (mas yr ⁻¹)	RV (km s ⁻¹)	[Fe/H] (dex)	Member Stars
NGC 6791	69.9658	+10.9080	6.3	4.42	7.70	-0.42 ± 0.25	-2.28 ± 0.29	-47.3 ± 1.4	$+0.42 \pm 0.05$	31
NGC 6819	73.9834	+8.4882	6.9	1.62	7.70	-2.92 ± 0.18	-3.86 ± 0.20	$+2.4 \pm 1.7$	$+0.11 \pm 0.03$	36
NGC 6811	79.2233	+12.0047	7.2	0.64	7.87	-3.39 ± 0.17	-8.78 ± 0.18	$+7.8 \pm 0.3$	-0.01 ± 0.02	4
Berkeley 53	90.3051	+3.7555	7.5	1.23	8.90	-3.77 ± 0.39	-5.69 ± 0.34	-36.3 ± 0.5	-0.00 ± 0.02	5
NGC 7789	115.5392	-5.3644	14.4	1.84	9.13	-0.93 ± 0.19	-1.93 ± 0.20	-54.7 ± 1.3	$+0.05 \pm 0.03$	17
FSR 0494	120.0882	+1.0206	5.7	2.00	10.60	-2.45 ± 0.48	-0.65 ± 0.48	-63.3 ± 1.5	$+0.01 \pm 0.02$	5
NGC 188	122.8416	+22.3840	17.7	4.47	9.06	-2.31 ± 0.19	-0.96 ± 0.16	-41.5 ± 1.1	$+0.14 \pm 0.03$	13
IC 166	130.0502	-0.1616	7.5	1.00	11.47	-1.46 ± 0.15	$+1.13 \pm 0.28$	-40.5 ± 1.5	-0.06 ± 0.02	15
Berkeley 66	139.4199	+0.1803	3.3	1.41	11.55	-0.14 ± 0.61	$+0.01 \pm 0.69$	-50.1 ± 0.3	-0.13 ± 0.02	6
King 5	143.7732	-4.2760	8.4	1.23	10.01	-0.26 ± 0.28	-1.16 ± 0.29	-44.3 ± 1.5	-0.11 ± 0.02	5
NGC 1245	146.6533	-8.9081	11.4	1.06	10.66	$+0.52 \pm 0.23$	-1.57 ± 0.19	-29.2 ± 0.8	-0.06 ± 0.02	23
King 7	149.7993	-1.0215	11.1	0.71	10.54	$+1.07 \pm 0.55$	-1.21 ± 0.42	-11.9 ± 2.0	-0.05 ± 0.02	4
NGC 1798	160.6994	+4.8502	5.4	2.00	12.50	$+0.89 \pm 0.33$	-0.33 ± 0.31	$+2.0 \pm 1.7$	-0.18 ± 0.02	9
Berkeley 17	175.6574	-3.6494	7.2	3.98	11.08	$+2.55 \pm 0.41$	-0.32 ± 0.27	-73.4 ± 0.4	-0.11 ± 0.03	7
Berkeley 71	176.6384	+0.8936	4.8	1.05	11.51	$+0.68 \pm 0.36$	-1.62 ± 0.46	-8.7 ± 2.3	-0.20 ± 0.03	7
Teutsch 51	182.7401	+0.4760	2.7	0.53	11.68	$+0.56 \pm 0.29$	-0.34 ± 0.34	$+17.0 \pm 1.4$	-0.28 ± 0.03	5
NGC 2158	186.6394	+1.7807	8.4	2.14	12.41	-0.18 ± 0.32	-2.01 ± 0.25	$+27.5 \pm 1.5$	-0.15 ± 0.03	18
NGC 2420	198.1134	+19.6318	7.5	2.32	10.25	-1.19 ± 0.22	-2.13 ± 0.18	$+74.2 \pm 0.5$	-0.12 ± 0.02	15
NGC 2682	215.6906	+31.9221	33.0	3.43	8.60	-10.97 ± 0.24	-2.95 ± 0.24	$+33.8 \pm 1.0$	$+0.07 \pm 0.03$	35

Notes.

^a From Kharchenko et al. (2013).

^b Calculated using Bailer-Jones et al. (2018) with a solar $R_{\text{GC}} = 8$ kpc.

^c μ_{α} and μ_{δ} and their 1σ uncertainties are those of the 2D Gaussian fit, discussed in Section 3.2.

^d A separate analysis of APOGEE data for the open cluster IC 166 found 13 member stars and an average [Fe/H] of -0.08 ± 0.05 . These results can be found in Schiappacasse-Ulloa et al. (2018).

We find the majority of clusters have an uncertainty of 0.02–0.03 dex, with the exception of one cluster (King 7), which has a standard deviation of only 0.01; we therefore enforce a more conservative 0.02 dex uncertainty for this cluster.

Our final sample, assuming a solar distance to the Galactic center of 8 kpc and using the median distance to likely members (stellar distances are taken from Bailer-Jones et al. 2018; this is discussed in detail in Section 5.3) is presented in Table 2.

4. Cluster Metallicities in Comparison to Previous Work

In order to place our results in the context of previous work, we conducted a detailed comparison of key well-studied clusters from the literature: NGC 188, NGC 2682 (M67), NGC 2420, NGC 6791, NGC 6819, and NGC 7789, presented in Figure 3 and discussed below.

4.1. NGC 2682 (M67)

Figure 3 shows that all of the literature values (Tautvaišiene et al. 2000; Yong et al. 2005; Friel et al. 2010; Pancino et al. 2010; Jacobson et al. 2011; Reddy et al. 2013; Casamiquela et al. 2017; OCCAM Paper III: O’Connell et al. 2018) for M67 agree within quoted uncertainties, except for the lowest metallicity value from Reddy et al. (2013), in which the authors note a possible metal-poor offset from the literature. The mean difference from the literature values is -0.06 ± 0.04 dex for this cluster.

4.2. NGC 188

We find that three studies (Friel et al. 2010; Overbeek et al. 2016; O’Connell et al. 2018) are in agreement with our results; however, we find significant differences with Jacobson et al. (2011) and Casamiquela et al. (2017). The mean

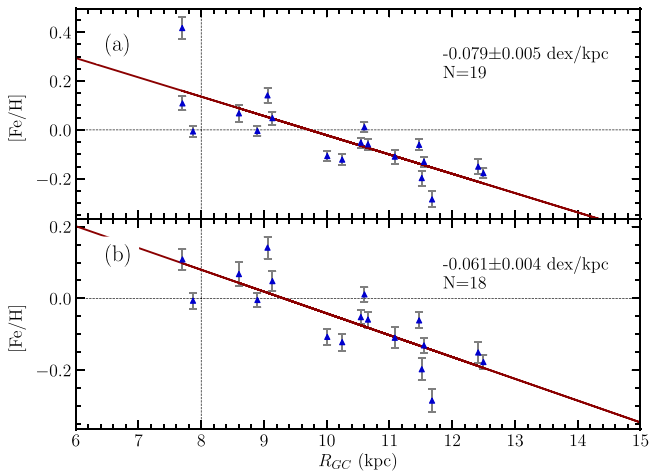


Figure 4. The high-reliability metallicity gradients using APOGEE clusters. Dotted lines are shown for reference at $R_{\odot} = 8$ kpc and $[\text{Fe}/\text{H}] = 0$ dex. Panel (a) shows the entire sample and panel (b) shows the sample with the very metal-rich NGC 6791 removed.

Table 3
 R_{GC} Calculated Using Different Distance Sources

Cluster name	R_{GC} Dias (kpc)	R_{GC} MWSC (kpc)	R_{GC} Parallax (kpc)	R_{GC} Bailer-Jones (kpc)
NGC 6791	7.83	7.80	7.57	7.70
NGC 6819	7.69	7.69	7.69	7.70
NGC 6811	7.86	7.86	7.87	7.87
Berkeley 53	8.59	8.67	8.67	8.90
NGC 7789	8.92	8.92	9.01	9.13
FSR 0494	11.43	11.43	10.14	10.60
NGC 188	9.17	9.14	8.96	9.06
IC 166	11.68	11.68	10.92	11.47
Berkeley 66	12.24	14.08	11.46	11.55
King 5	9.88	9.86	9.79	10.01
NGC 1245	10.44	10.60	10.32	10.66
King 7	9.96	10.36	10.22	10.54
NGC 1798	12.39	13.05	11.68	12.50
Berkeley 17	10.69	9.79	10.68	11.08
Berkeley 71	11.26	11.26	11.03	11.51
Teutsch 51	11.30	11.78	11.20	11.68
NGC 2158	13.05	12.75	11.70	12.41
NGC 2420	10.25	10.61	10.04	10.25
NGC 2682	8.57	8.62	8.58	8.60

difference from the literature is -0.09 ± 0.06 dex for this cluster, the highest of the commonly studied clusters analyzed.

4.3. NGC 6791

We find general agreement with all but one of the literature values considered (Casamiquela et al. 2017, finds a significantly lower metallicity), and note the majority of literature values (Carraro et al. 2006; Origlia et al. 2006; Carretta et al. 2007; Bragaglia et al. 2014; Cunha et al. 2015; O’Connell et al. 2018) again fall slightly below ours, with a mean difference from the literature of -0.06 ± 0.08 dex. We hypothesize that this may be due to a poor calibration in the metal-rich end of the APOGEE calibrations. Cunha et al.

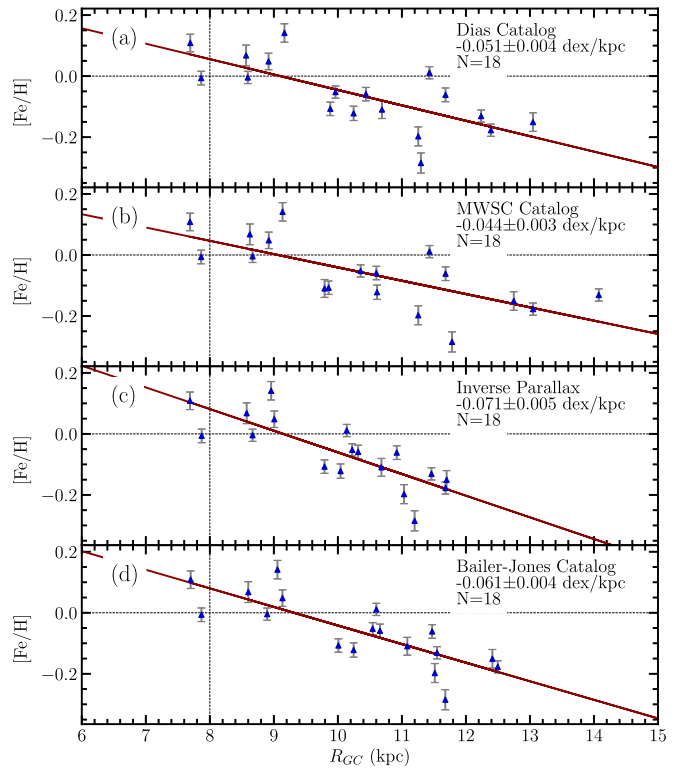


Figure 5. The galactic metallicity gradient computed using values from the Dias Catalog (Dias et al. 2002), the MWSC Catalog (Kharchenko et al. 2013), inverse-parallax (Gaia Collaboration et al. 2018; Lindegren et al. 2018), and the Bailer-Jones catalog (Bailer-Jones et al. 2018).

Table 4
A Summary of Reported Spectroscopic Metallicity Gradients

Study	dex kpc ⁻¹	# Study	# Total	Range kpc
Carraro et al. (1998)	-0.085 ± 0.008	0	37	7–16
Friel et al. (2002)	-0.06 ± 0.01	24	39	7–16
Carrera & Pancino (2011) ^a	-0.070 ± 0.010	9	89	6–12.5
Jacobson et al. (2011)	-0.085 ± 0.019	10	19	9–13
Yong et al. (2012) ^a	-0.09 ± 0.01	5	49	6–13
Reddy et al. (2016) ^a	-0.052 ± 0.011	28	79	5–12
This Study	-0.061 ± 0.004	18	18	7–12

Notes. The number of clusters studied by the authors is given, as well as the total number of clusters (including those drawn from the literature) used for the measurement. The range of R_{GC} covered is given, as well as the point at which the authors split their two-function gradient (if any). Studies that included only very young or very old clusters are excluded, as were studies that covered a significantly different range in R_{GC} .

^a These studies fit a two-function gradient. We quote only the gradient measured for the inner sample, as we only discuss this measurement.

(2015) found a lower metallicity ($[\text{Fe}/\text{H}] = 0.34 \pm 0.06$) using APOGEE spectra of many of the same stars for a detailed individual analysis, as compared with our DR14 pipeline value ($[\text{Fe}/\text{H}] = 0.42 \pm 0.05$). We note, however, that Cunha et al. (2015) used an older version of the ASPCAP line list and the DR14 ASPCAP results, and that the Cunha et al. (2015) results agree within the uncertainties given the changes in the line list.

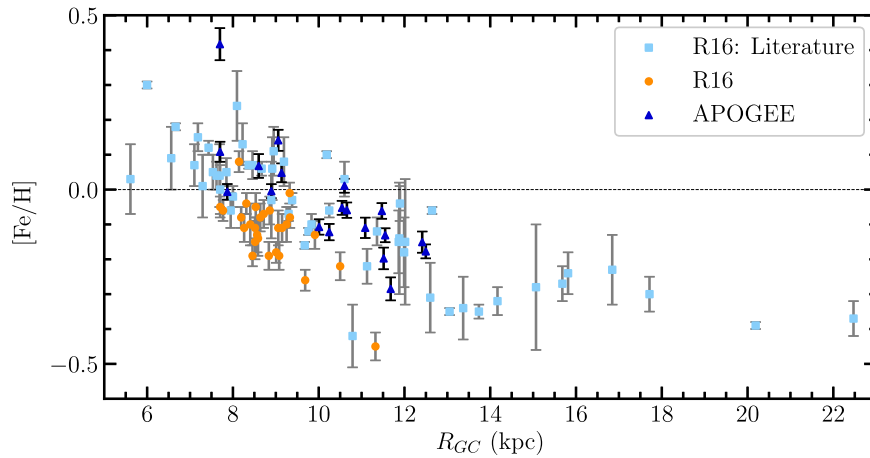


Figure 6. The Galactic abundance trend (R_{GC} vs. $[Fe/H]$) assuming $R_{GC,\odot} = 8.0$ kpc. Our sample (dark blue triangles) is shown along with a literature sample from Reddy et al. (2016) (light blue points), and clusters analyzed by Reddy et al. (2012, 2013, 2015, 2016) (orange points).

4.4. NGC 2420, NGC 6819, and NGC 7789

Nearly all of the literature results are in good agreement with ours, with the exception of Pancino et al. (2010) for NGC 2420, which quotes particularly small errors. The other results (Jacobson et al. 2011; Casamiquela et al. 2017; O’Connell et al. 2018) are consistent, and we note in particular the agreement with Souto et al. (2016), who completed a by-hand analysis of the same APOGEE spectra. The mean differences from the literature are -0.02 ± 0.05 , -0.05 ± 0.04 , and -0.03 ± 0.04 for NGC 2420, NGC 6819 (Bragaglia et al. 2001; Casamiquela et al. 2017; O’Connell et al. 2018), and NGC 7789 (Tautvaišienė et al. 2000; Pancino et al. 2010; Jacobson et al. 2011; Overbeek et al. 2016; Casamiquela et al. 2017; O’Connell et al. 2018), respectively.

4.5. APOGEE DR14 versus Literature Trends

The comparison for NGC 188, NGC 6791, and NGC 2682 clearly shows the majority of literature values are more metal-poor than our adopted values. The other clusters agree on the direction of the offset but suggest that it is not severe. Jönsson et al. (2018) compared to optical studies for 525 stars in common with APOGEE. They find an average difference (in the sense APOGEE—literature) of -0.04 ± 0.010 dex. From our comparison of 6 open clusters to 17 studies in the literature (Figure 3), we find a mean difference (in the sense APOGEE—literature) of -0.05 ± 0.06 . Both our analysis and the analysis of Jönsson et al. (2018) suggest the possibility of a *slight* global metal-rich offset in the APOGEE DR14 sample, but both analyses are consistent with no offset from the literature. Still, we emphasize that when using only the APOGEE DR14 sample for analysis, any global offset, minor or otherwise, will have no significant effect on the results of a *gradient* measurement.

5. Galactic Metallicity Gradients

The uniform OCCAM sample of 259 member stars in 19 open clusters was used to measure the Galactic metallicity gradient. The sample covers the disk from $R_{GC} \approx 7$ to 13 kpc with no major gaps.

In addition to uniform abundances, a uniform R_{GC} analysis is desirable. We considered four sources for cluster distances,

discussed in detail in Section 5.3. We use distances computed from the Bailer-Jones Catalog (Bailer-Jones et al. 2018) for the gradients we present below.

5.1. Error Analysis

The scatter in the abundance gradients necessitates some reliable determination of the uncertainty in any quoted gradient. A re-sampling routine is used to estimate the error in gradients. The gradient is determined 2000 times, each time using a randomly determined $[Fe/H]$ for each cluster, sampled from a standard normal distribution within their uncertainties. The mean of the resulting sample of 2000 gradients is adopted, and the standard deviation is taken as the uncertainty. A check was made against the χ^2 minimum error for a straight line fit in each case; it was found that in every case, our error estimation was larger than this minimum. These are the uncertainties quoted for all the gradients we present.

5.2. NGC 6791 and the Metallicity Gradient

The overall metallicity gradient with the entire sample included, is found to be -0.079 ± 0.005 dex kpc^{-1} (Figure 4(a)). We note that NGC 6791 is very metal-rich, fairly old, and relatively far from the Galactic plane. Previous work using APOGEE data has suggested it likely migrated to its current location (Linden et al. 2017). Since it is likely not representative of the region of the Galaxy in which it currently resides, we exclude it from further analysis. Previous work, including NGC 6791 such as Carraro et al. (1998) and Friel et al. (2002), used a much lower value for $[Fe/H]$ (+0.19 dex and +0.11 dex, respectively), low enough to be in disagreement with most recent studies. Even R16 used a lower value for NGC 6791 (+0.24 dex). Jacobson et al. (2011) note that it strongly influences the gradient.

Removing NGC 6791 gives a final metallicity gradient, from the full OCCAM high-reliability sample, of -0.061 ± 0.004 dex kpc^{-1} (Figure 4(b)).

5.3. Distance Effects on the Gradient

The metallicity gradients are highly susceptible to systematic differences in the distance values used. We considered four sources of distances: (1) the Dias Catalog (Dias et al. 2002),

Table 5
OCCAM DR14 Cluster Abundances

Cluster Name	[O/Fe] (dex)	[Mg/Fe] (dex)	[Si/Fe] (dex)	[S/Fe] (dex)	[Ca/Fe] (dex)	[V/Fe] (dex)	[Cr/Fe] (dex)	[Mn/Fe] (dex)	[Co/Fe] (dex)	[Ni/Fe] (dex)
NGC 6791	0.07 ± 0.04	0.06 ± 0.06	-0.01 ± 0.05	0.05 ± 0.11	0.02 ± 0.06	-0.01 ± 0.16	-0.11 ± 0.08	-0.00 ± 0.14	0.04 ± 0.27	-0.00 ± 0.04
NGC 6819	-0.02 ± 0.03	0.00 ± 0.02	0.00 ± 0.03	-0.02 ± 0.05	0.01 ± 0.02	0.02 ± 0.07	0.02 ± 0.03	0.03 ± 0.02	0.05 ± 0.08	0.02 ± 0.02
NGC 6811	-0.09 ± 0.04	-0.02 ± 0.02	0.00 ± 0.03	0.05 ± 0.05	-0.00 ± 0.03	-0.05 ± 0.08	0.01 ± 0.04	-0.00 ± 0.02	-0.21 ± 0.12	-0.02 ± 0.02
Berkeley 53	-0.02 ± 0.03	-0.02 ± 0.02	0.01 ± 0.03	0.03 ± 0.06	0.01 ± 0.03	0.00 ± 0.08	-0.03 ± 0.04	-0.01 ± 0.03	-0.31 ± 0.30	-0.02 ± 0.02
NGC 7789	-0.03 ± 0.03	-0.02 ± 0.02	-0.02 ± 0.02	-0.00 ± 0.05	-0.02 ± 0.02	-0.01 ± 0.09	0.00 ± 0.05	-0.01 ± 0.02	-0.07 ± 0.09	-0.03 ± 0.02
FSR 0494	-0.05 ± 0.05	-0.04 ± 0.02	-0.02 ± 0.03	-0.01 ± 0.08	-0.00 ± 0.04	0.12 ± 0.11	0.03 ± 0.06	0.02 ± 0.04	0.05 ± 0.22	0.01 ± 0.03
NGC 188	0.02 ± 0.04	0.05 ± 0.02	0.01 ± 0.02	0.01 ± 0.08	-0.02 ± 0.02	0.03 ± 0.08	-0.01 ± 0.06	0.08 ± 0.03	0.13 ± 0.11	0.04 ± 0.02
IC 166	-0.02 ± 0.07	0.02 ± 0.04	0.07 ± 0.06	0.04 ± 0.14	-0.00 ± 0.04	-0.12 ± 0.27	0.00 ± 0.06	0.00 ± 0.04	-0.41 ± 0.60	-0.02 ± 0.03
Berkeley 66	0.04 ± 0.10	0.06 ± 0.03	0.05 ± 0.03	0.01 ± 0.07	-0.00 ± 0.04	-0.14 ± 0.17	0.01 ± 0.06	-0.05 ± 0.04	-0.01 ± 0.22	-0.03 ± 0.05
King 5	0.00 ± 0.04	-0.02 ± 0.02	0.03 ± 0.03	0.07 ± 0.06	-0.00 ± 0.03	-0.01 ± 0.11	0.04 ± 0.04	-0.03 ± 0.04	-0.00 ± 0.12	-0.01 ± 0.02
NGC 1245	-0.03 ± 0.07	-0.03 ± 0.02	0.03 ± 0.03	0.00 ± 0.07	-0.00 ± 0.03	0.04 ± 0.09	0.01 ± 0.05	-0.01 ± 0.03	-0.17 ± 0.50	-0.04 ± 0.02
King 7	-0.02 ± 0.03	-0.01 ± 0.02	0.04 ± 0.03	0.10 ± 0.07	0.00 ± 0.02	-0.06 ± 0.07	0.03 ± 0.03	0.03 ± 0.03	-0.04 ± 0.07	-0.05 ± 0.02
NGC 1798	0.01 ± 0.06	-0.01 ± 0.02	0.01 ± 0.03	0.01 ± 0.06	0.03 ± 0.03	-0.03 ± 0.11	-0.00 ± 0.05	-0.07 ± 0.03	-0.18 ± 0.25	-0.03 ± 0.02
Berkeley 17	0.03 ± 0.03	0.06 ± 0.02	0.02 ± 0.03	0.06 ± 0.05	0.01 ± 0.03	0.02 ± 0.07	0.03 ± 0.04	-0.01 ± 0.03	0.06 ± 0.07	0.03 ± 0.02
Berkeley 71	0.02 ± 0.09	0.03 ± 0.05	0.06 ± 0.03	0.13 ± 0.08	0.03 ± 0.03	0.03 ± 0.11	0.01 ± 0.07	-0.04 ± 0.04	-0.14 ± 0.23	-0.03 ± 0.02
Teutsch 51	0.08 ± 0.08	0.01 ± 0.03	0.06 ± 0.06	0.01 ± 0.13	0.03 ± 0.05	-0.00 ± 0.13	0.05 ± 0.08	-0.03 ± 0.05	0.09 ± 0.21	-0.01 ± 0.04
NGC 2158	0.00 ± 0.07	0.03 ± 0.02	0.03 ± 0.03	0.10 ± 0.09	-0.00 ± 0.03	-0.15 ± 0.13	-0.07 ± 0.12	-0.05 ± 0.04	-0.07 ± 0.22	-0.01 ± 0.03
NGC 2420	0.05 ± 0.06	0.00 ± 0.03	0.01 ± 0.03	-0.01 ± 0.06	0.03 ± 0.03	-0.09 ± 0.13	-0.04 ± 0.10	-0.04 ± 0.03	-0.18 ± 0.20	-0.02 ± 0.02
NGC 2682	-0.03 ± 0.04	0.01 ± 0.02	-0.03 ± 0.02	-0.02 ± 0.05	-0.02 ± 0.02	-0.08 ± 0.13	-0.02 ± 0.07	0.01 ± 0.02	-0.00 ± 0.09	0.02 ± 0.02

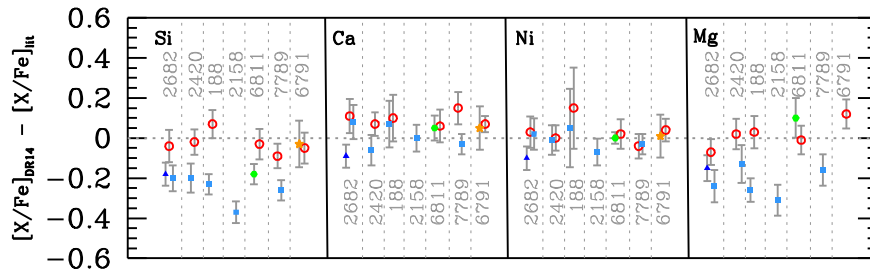


Figure 7. Comparison of individual elemental abundances using the APOGEE calibration clusters with available comparison elements in the other literature studies. Clusters are color-coded by analysis group: *dark blue* for Reddy et al. (2013, 2016), *light blue* for Jacobson et al. (2011), *green* for Bragaglia et al. (2001), *orange* for Carraro et al. (2006), and *red* for O’Connell et al. (2018).

Table 6
DR14 OCAAM Open Cluster Member Star Abundances

Cluster	2MASS ID	RV (km s ⁻¹)	[Fe/H] (dex)	[O/Fe] (dex)	[Mg/Fe] (dex)	[Ca/Fe] (dex)	[Si/Fe] (dex)	[S/Fe] (dex)
				[V/Fe] (dex)	[Cr/Fe] (dex)	[Mn/Fe] (dex)	[Co/Fe] (dex)	[Ni/Fe] (dex)
NGC 6819	2M19404803+4008085	2.4 ± 0.1	0.09 ± 0.01	-0.01 ± 0.02	0.02 ± 0.02	0.01 ± 0.02	0.02 ± 0.02	-0.00 ± 0.05
				0.04 ± 0.06	0.02 ± 0.03	0.01 ± 0.02	0.07 ± 0.06	0.01 ± 0.01
NGC 6819	2M19404965+4014313	3.1 ± 0.0	0.12 ± 0.01	0.01 ± 0.03	0.01 ± 0.02	0.02 ± 0.02	0.00 ± 0.02	-0.03 ± 0.05
				0.06 ± 0.07	0.02 ± 0.04	0.03 ± 0.03	0.07 ± 0.08	0.02 ± 0.02
NGC 6819	2M19405020+4013109	4.3 ± 0.0	0.15 ± 0.01	0.00 ± 0.03	0.00 ± 0.02	-0.00 ± 0.02	-0.04 ± 0.02	-0.04 ± 0.05
				-0.02 ± 0.06	-0.02 ± 0.03	0.01 ± 0.02	0.03 ± 0.07	0.02 ± 0.01
NGC 6819	2M19405601+4013395	3.3 ± 0.1	0.09 ± 0.01	0.04 ± 0.04	-0.00 ± 0.02	0.02 ± 0.03	-0.13 ± 0.03	-0.07 ± 0.06
				-0.01 ± 0.09	-0.00 ± 0.05	0.02 ± 0.03	0.10 ± 0.10	0.00 ± 0.02
NGC 6819	2M19405797+4008174	4.5 ± 0.1	0.13 ± 0.01	0.00 ± 0.03	0.02 ± 0.02	0.00 ± 0.02	0.01 ± 0.02	-0.06 ± 0.05
				0.08 ± 0.07	0.03 ± 0.03	0.05 ± 0.02	0.03 ± 0.07	0.00 ± 0.01
NGC 6819	2M19410524+4014042	3.3 ± 0.1	0.14 ± 0.01	-0.03 ± 0.03	-0.01 ± 0.02	0.04 ± 0.02	0.02 ± 0.03	0.03 ± 0.05
				0.02 ± 0.07	0.02 ± 0.04	0.03 ± 0.03	-0.04 ± 0.08	0.04 ± 0.02
NGC 6819	2M19410622+4010532	3.2 ± 0.0	0.12 ± 0.01	0.07 ± 0.04	0.01 ± 0.02	0.02 ± 0.03	0.03 ± 0.03	-0.05 ± 0.06
				0.02 ± 0.08	-0.04 ± 0.04	0.02 ± 0.03	0.03 ± 0.10	0.02 ± 0.02
NGC 6819	2M19410858+4013299	2.3 ± 0.0	0.11 ± 0.01	-0.06 ± 0.03	0.00 ± 0.02	-0.01 ± 0.02	0.03 ± 0.02	-0.03 ± 0.05
				0.03 ± 0.06	0.03 ± 0.03	0.03 ± 0.02	0.08 ± 0.07	0.01 ± 0.01
NGC 6819	2M19410926+4014436	2.3 ± 0.1	0.13 ± 0.01	-0.03 ± 0.03	0.00 ± 0.02	-0.00 ± 0.02	-0.03 ± 0.02	-0.02 ± 0.05
				-0.04 ± 0.06	-0.00 ± 0.03	0.00 ± 0.02	0.01 ± 0.07	-0.02 ± 0.01
NGC 6819	2M19410991+4015495	2.5 ± 0.1	0.07 ± 0.01	-0.03 ± 0.03	-0.00 ± 0.02	0.05 ± 0.02	0.01 ± 0.03	0.02 ± 0.05
				0.13 ± 0.07	0.06 ± 0.04	0.00 ± 0.03	0.13 ± 0.08	0.03 ± 0.02

(This table is available in its entirety in machine-readable form.)

which is a compilation of distances from the literature, (2) the MWSC Catalog (Kharchenko et al. 2013), which recomputed distances to each cluster, (3) inverse-parallax (Gaia Collaboration et al. 2018; Lindegren et al. 2018), accounting for a 0.08 mas offset (Stassun & Torres 2018), and (4) the Bailer-Jones catalog (Bailer-Jones et al. 2018), which used the same parallax measurements combined with a geometric prior to compute distances to nearly every star in *Gaia* DR2. Table 3 shows a summary of R_{GC} using these four sources for distance, while Figure 5 shows the $d[Fe/H]/dR_{GC}$ gradient computed using different distance catalogs/methods.

Not surprisingly, the parallax and Bailer-Jones distances are fairly similar, at least for relatively nearby clusters, yet still, the gradient measurements are incompatible. The Dias Catalog and MWSC Catalog distances are similar for a number of clusters, but for clusters at higher R_{GC} , they tend to be larger than Bailer-Jones or parallax, leading to a shallower gradient result for both catalogs. The Dias Catalog and MWSC Catalog gradients are barely in agreement within the uncertainties.

The MWSC Catalog recomputed distances for every cluster and thus is internally consistent. The parallax distances and

Bailer-Jones distances are internally consistent as well. But there is a clear discrepancy between these three data sets. The Bailer-Jones geometric distances should be the most accurate for nearby clusters, since they are based on *Gaia* parallaxes. Considering clusters within $7 \text{ kpc} < R_{GC} < 10 \text{ kpc}$, the MWSC Catalog distances are in good agreement with Bailer-Jones distances. For some more distant clusters, significant discrepancies exist (e.g., Berkeley 66 and Berkeley 17), while many remain in good agreement. At this time, we have no strong evidence to distrust one catalog over the other at larger distances, but a decision must be made. Looking at the two clusters with very discrepant MWSC Catalog distances (Berkeley 66 and Berkeley 17), we see they also disagree significantly with the Dias Catalog, so for this study, we adopt distances calculated from the Bailer-Jones Catalog.

5.4. Comparison to Previous Work

A summary of current results in the literature (from studies using high-resolution spectroscopy) is found in Table 4. We omit studies that measure a gradient in a region significantly

Table 7
DR14 OCCAM Abundance Comparison to Literature

Cluster	Abundance Lit. (dex)	# Cluster Stars Lit.	Abundance DR 14 (dex)	# Cluster Stars DR14	$\Delta[X/Fe]$ (dex)	References
[Si/Fe]						
NGC 6819	+0.18 ± 0.04	3	+0.00 ± 0.03	36	-0.18 ± 0.05	Bragaglia et al. (2001)
NGC 6819	+0.03 ± 0.07	3	+0.00 ± 0.03	36	-0.03 ± 0.08	O'Connell et al. (2018)
NGC 6791	+0.02 ± 0.10	10	-0.01 ± 0.06	31	-0.03 ± 0.12	Carraro et al. (2006)
NGC 6791	+0.04 ± 0.05	2	-0.01 ± 0.06	31	-0.05 ± 0.08	O'Connell et al. (2018)
NGC 2158	+0.39 ± 0.05	15	+0.02 ± 0.02	18	-0.37 ± 0.05	Jacobson et al. (2009)
NGC 188	+0.25 ± 0.05	27	+0.02 ± 0.01	13	-0.23 ± 0.05	Jacobson et al. (2011)
NGC 188	-0.05 ± 0.07	3	+0.02 ± 0.01	13	+0.07 ± 0.07	O'Connell et al. (2018)
NGC 2420	+0.21 ± 0.07	9	+0.01 ± 0.02	15	-0.20 ± 0.07	Jacobson et al. (2011)
NGC 2420	+0.03 ± 0.06	6	+0.01 ± 0.02	15	-0.02 ± 0.06	O'Connell et al. (2018)
NGC 2682	+0.21 ± 0.05	19	+0.01 ± 0.04	35	-0.20 ± 0.06	Jacobson et al. (2011)
NGC 2682	+0.19 ± 0.04	3	+0.01 ± 0.04	35	-0.18 ± 0.06	Reddy et al. (2013)
NGC 2682	+0.05 ± 0.07	10	+0.01 ± 0.04	35	-0.04 ± 0.08	O'Connell et al. (2018)
NGC 7789	+0.25 ± 0.05	28	-0.01 ± 0.01	17	-0.26 ± 0.05	Jacobson et al. (2011)
NGC 7789	+0.08 ± 0.06	5	-0.01 ± 0.01	17	-0.09 ± 0.06	O'Connell et al. (2018)
[Ca/Fe]						
NGC 6819	-0.04 ± 0.06	3	+0.01 ± 0.02	36	+0.05 ± 0.06	Bragaglia et al. (2001)
NGC 6819	-0.05 ± 0.08	3	+0.01 ± 0.02	36	+0.06 ± 0.08	O'Connell et al. (2018)
NGC 6791	-0.03 ± 0.10	10	+0.02 ± 0.04	31	+0.05 ± 0.11	Carraro et al. (2006)
NGC 6791	-0.05 ± ...	2	+0.02 ± 0.04	31	+0.07 ± ...	O'Connell et al. (2018)
NGC 2158	+0.00 ± 0.06	15	+0.00 ± 0.03	18	+0.00 ± 0.07	Jacobson et al. (2009)
NGC 188	-0.04 ± 0.06	27	+0.03 ± 0.10	13	+0.07 ± 0.12	Jacobson et al. (2011)
NGC 188	-0.07 ± 0.06	3	+0.03 ± 0.10	13	+0.10 ± 0.12	O'Connell et al. (2018)
NGC 2420	+0.10 ± 0.07	9	+0.04 ± 0.03	15	-0.06 ± 0.08	Jacobson et al. (2011)
NGC 2420	-0.03 ± 0.05	6	+0.04 ± 0.03	15	+0.07 ± 0.06	O'Connell et al. (2018)
NGC 2682	-0.11 ± 0.07	19	-0.03 ± 0.05	35	+0.08 ± 0.09	Jacobson et al. (2011)
NGC 2682	+0.06 ± 0.03	3	-0.03 ± 0.05	35	-0.09 ± 0.06	Reddy et al. (2013)
NGC 2682	-0.14 ± 0.07	10	-0.03 ± 0.05	35	+0.11 ± 0.09	O'Connell et al. (2018)
NGC 7789	+0.01 ± 0.05	28	-0.02 ± 0.01	17	-0.03 ± 0.05	Jacobson et al. (2011)
NGC 7789	-0.17 ± 0.08	5	-0.02 ± 0.01	17	+0.15 ± 0.08	O'Connell et al. (2018)
[Ni/Fe]						
NGC 6819	+0.01 ± 0.02	3	+0.01 ± 0.02	36	+0.00 ± 0.03	Bragaglia et al. (2001)
NGC 6819	-0.01 ± 0.07	3	+0.01 ± 0.02	36	+0.02 ± 0.07	O'Connell et al. (2018)
NGC 6791	-0.01 ± 0.10	10	+0.00 ± 0.04	31	+0.01 ± 0.11	Carraro et al. (2006)
NGC 6791	-0.04 ± 0.04	2	+0.00 ± 0.04	31	+0.04 ± 0.06	O'Connell et al. (2018)
NGC 2158	+0.05 ± 0.06	15	-0.02 ± 0.03	18	-0.07 ± 0.07	Jacobson et al. (2009)
NGC 188	+0.08 ± 0.05	27	+0.13 ± 0.19	13	+0.05 ± 0.20	Jacobson et al. (2011)
NGC 188	-0.02 ± 0.07	3	+0.13 ± 0.19	13	+0.15 ± 0.20	O'Connell et al. (2018)
NGC 2420	-0.01 ± 0.07	9	-0.02 ± 0.02	15	-0.01 ± 0.07	Jacobson et al. (2011)
NGC 2420	-0.02 ± 0.06	6	-0.02 ± 0.02	15	-0.00 ± 0.06	O'Connell et al. (2018)
NGC 2682	-0.01 ± 0.06	19	+0.01 ± 0.05	35	+0.02 ± 0.08	Jacobson et al. (2011)
NGC 2682	+0.11 ± 0.03	3	+0.01 ± 0.05	35	-0.10 ± 0.06	Reddy et al. (2013)
NGC 2682	-0.02 ± 0.06	10	+0.01 ± 0.05	35	+0.03 ± 0.08	O'Connell et al. (2018)
NGC 7789	+0.00 ± 0.05	28	-0.03 ± 0.01	17	-0.03 ± 0.05	Jacobson et al. (2011)
NGC 7789	+0.01 ± 0.06	5	-0.03 ± 0.01	17	-0.04 ± 0.06	O'Connell et al. (2018)
[Mg/Fe]						
NGC 6819	-0.12 ± 0.07	3	+0.00 ± 0.01	36	+0.12 ± 0.07	Bragaglia et al. (2001)
NGC 6819	+0.01 ± 0.07	3	+0.00 ± 0.01	36	-0.01 ± 0.07	O'Connell et al. (2018)
NGC 2158	+0.22 ± 0.07	15	+0.03 ± 0.01	18	-0.19 ± 0.07	Jacobson et al. (2009)
NGC 188	+0.26 ± 0.05	27	+0.03 ± 0.04	13	-0.23 ± 0.06	Jacobson et al. (2011)
NGC 188	+0.00 ± 0.07	3	+0.03 ± 0.04	13	+0.03 ± 0.08	O'Connell et al. (2018)
NGC 2420	+0.11 ± 0.09	9	+0.00 ± 0.03	15	-0.11 ± 0.09	Jacobson et al. (2011)
NGC 2420	-0.02 ± 0.07	6	+0.00 ± 0.03	15	+0.02 ± 0.08	O'Connell et al. (2018)
NGC 2682	+0.23 ± 0.07	19	-0.03 ± 0.05	35	-0.26 ± 0.09	Jacobson et al. (2011)
NGC 2682	+0.12 ± 0.04	3	-0.03 ± 0.05	35	-0.16 ± 0.06	Reddy et al. (2013)
NGC 2682	+0.04 ± 0.04	10	-0.03 ± 0.05	35	-0.07 ± 0.06	O'Connell et al. (2018)
NGC 7789	+0.14 ± 0.05	28	-0.02 ± 0.01	17	-0.16 ± 0.05	Jacobson et al. (2011)
NGC 7789	-0.07 ± 0.04	5	-0.02 ± 0.01	17	+0.05 ± 0.04	O'Connell et al. (2018)

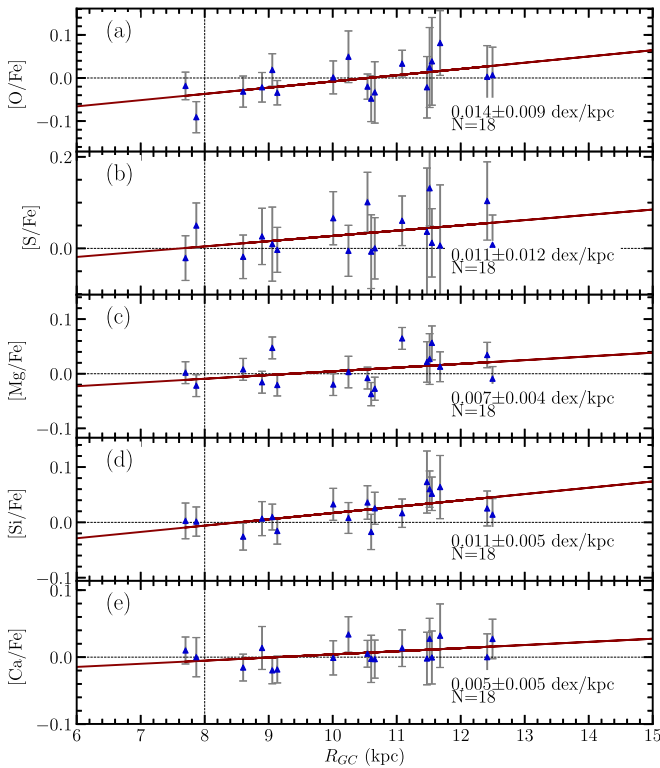


Figure 8. Galactic trend for our sample for the α elements (O, S, Mg, Si, Ca) from DR14.

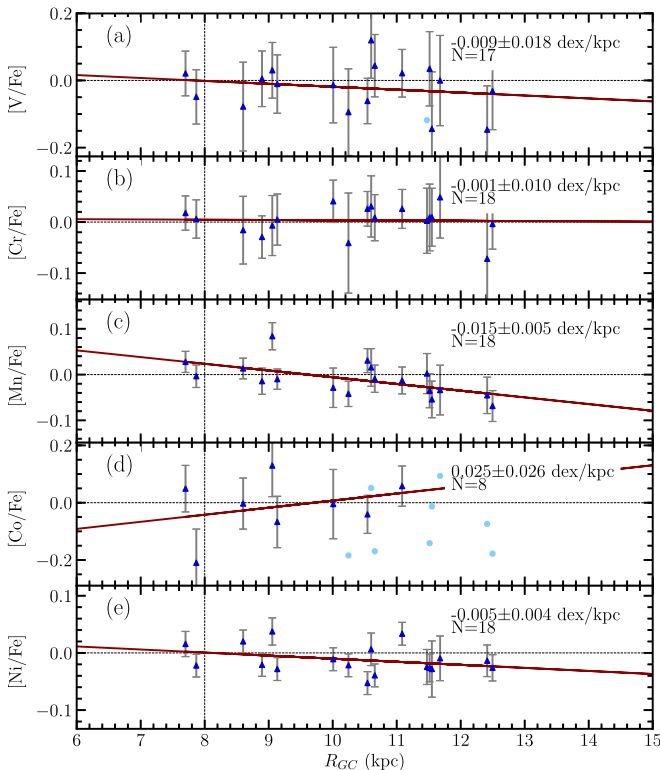


Figure 9. Galactic trend for our sample for the iron-peak (V, Co, Mn, Cr, Ni) elements from DR14. Clusters with very large uncertainties are not included in the fit (N reflects only those included in the fit), but are shown for reference as blue dots.

different than that considered in this paper. We can readily compare the APOGEE metallicity gradients to these results.

5.4.1. Comparison to APOGEE DR12

We recomputed the metallicity gradient found from APOGEE DR12 (Cunha et al. 2016) using only clusters in common with this work (and excluding NGC 6791) and distances from Dias et al. (2002) and found a gradient of -0.035 ± 0.014 . This agrees within the uncertainties with our gradient measured using the Dias catalog. The differences between the metallicity gradients can be explained in terms of improvements in the data reduction of APOGEE spectra, line list, and methodology (Holtzman et al. 2018).

5.4.2. Comparison to the Other Work

We find a metallicity gradient consistent with four of the six studies, the two discrepant results being Carraro et al. (1998) and Yong et al. (2012), which both quote particularly steep gradients. We find a relatively close agreement with Friel et al. (2002), Carrera & Pancino (2011), and R16. We note that if we instead compare the metallicity gradient computed with NGC 6791, our result is in agreement with Carraro et al. (1998) and Yong et al. (2012), but would no longer be in agreement with R16 or Friel et al. (2002). It is worth emphasizing that R16 and Friel et al. (2002) both had large uniform samples (24 and 28 open clusters, respectively) in addition to the literature samples included in their studies. Since the R16 study is both recent and very large, we compare to it directly. In Figure 6, we show the sample uniformly analyzed in R16 (orange points) and their literature-compiled sample (light blue points), along with the APOGEE results (dark blue triangles).

6. Other Elements Beyond [Fe/H]

We compute mean DR14 cluster abundances for reliable α -related elements (O, Ca, Mg, Si, S) and iron-peak elements (Cr, Co, Ni, Mn, V) in the same manner as [Fe/H], shown in Table 5. The abundances are shown for individual stars in Table 6.

6.1. OCCAM DR14 Calibration Sample

We use the APOGEE calibration cluster set to search for systematics in other available elements (Si, Ca, Ni, Mg). As shown in Figure 7 and listed in Table 7, there are no significant systematic offsets, with the possible exception of [Mg/Fe] and [Si/Fe]. For all other elements, the offsets are within the uncertainties (see Section 5.1) for nearly every study and cluster. Jönsson et al. (2018) also perform a detailed comparison to the literature for these elements, and find no significant systematic offsets. For [Mg/Fe], the APOGEE data are offset from the Jacobson et al. (2011) clusters, but not from Bragaglia et al. (2001) and Carraro et al. (2006) data. These [Mg/Fe] discrepancies are most likely due to line-list differences and will require further exploration; however, since we are consistent with some clusters and likely the effect is systematic between groups, we apply no offset here.

6.2. Galactic Gradients in Other Elements

The full APOGEE DR14 sample allows an exploration of individual abundance gradients for key element groups,¹⁶ such as α -related elements and iron-peak elements. These elements are key for exploring how Galactic chemical enrichment occurs, as each element is produced in a different manner (e.g., SNII versus SNIa yield ratios).

We find statistically significant *increasing* trends for some of the α elements ([O/Fe], [Mg/Fe], and [Si/Fe]), seen in Figure 8. The other α trends (Si, Ca) also show a positive trend, but their large uncertainties make them also consistent with a slope of zero. This behavior is consistent with previous work (e.g., Jacobson et al. 2011), which also found a significant $d[\text{O}/\text{Fe}]/dR$ trend from a literature-compiled cluster sample.

This mild positive $[\alpha/\text{Fe}]$ gradient is in agreement with the chemical evolution models of Minchev et al. (2014), who find an [Mg/Fe] gradient (averaged over all age ranges, for $|Z| < 0.25$ kpc) of $0.009 \text{ dex kpc}^{-1}$, although the gradient for younger populations (which may better match our relatively young sample) is steeper, e.g., $0.027 \text{ dex kpc}^{-1}$ for age < 2 Gyr. The models of Kubryk et al. (2015) also show a qualitatively similar trend for [O/Fe].

We also see a statistically significant *decreasing* trend for the iron-peak elements [Mn/Fe] and [Ni/Fe] as seen in Figure 9. The uncertainties are too large to draw meaningful conclusions for other elements (V, Cr, Co).

7. Conclusions

We describe the technique used by the OCCAM survey for targeting likely open cluster members, and another technique for determining the likelihood of their membership in a cluster. Using the determined likely cluster giant members, we present the first multi-element data from the OCCAM collaboration's exploration of the SDSS/APOGEE open cluster data presented in DR14.

We present abundance measurements of 11 elements for 19 open clusters and find no systematic offsets from previous work in the literature. Using distance measurements from Bailer-Jones et al. (2018), we make measurements of the Galactic abundance gradient for all 11 elements. Our results are in general agreement with previous work, and we present new evidence for a trend in [Mn/Fe] and [Ni/Fe]. Specifically:

1. The [Fe/H] gradient is $-0.061 \pm 0.004 \text{ dex kpc}^{-1}$, derived from clusters spanning $7 < R_{GC} < 13$ kpc.
2. We measure a mild $[\alpha/\text{Fe}]$ gradient, including [O/Fe], [Mg/Fe], and [Si/Fe], and mild negative gradient for the iron-peak elements [Mn/Fe] and [Ni/Fe].

While our sample of 19 open clusters is one of the largest *uniform* samples to date used to study Galactic abundance gradients, it is still small. Nevertheless, our results show tight correlations with a linear fit and good agreement with previous work in the literature, suggesting that APOGEE data can be a powerful tool in studying Galactic abundance gradients. Future work will feature more clusters from larger number of open clusters observed by APOGEE and comparisons with chemical evolution and chemodynamical models.

¹⁶ While the DR14 APOGEE sample also contains C and N, these elements have strong stellar evolutionary changes along the giant branch. Given the small numbers of stars per cluster, we have excluded these elements from consideration in this paper.

J.D., P.M.F., B.T., J.O., K.M.J., and B.M.M. acknowledge support for this research from the National Science Foundation (AST-1311835 & AST-1715662) and the TCU RCAF and JFSRP programs. K.M.J. also acknowledges funding from a TCU SERC grant and NSF REU (PHY-0851558). K.C. acknowledges support for this research from the National Science Foundation (AST-0907873). D.A.G.H. and O.Z. acknowledge support provided by the Spanish Ministry of Economy and Competitiveness (MINECO) under grant AYA-2017-88254-P. We would like to thank J. G. Fernández-Trincado and Doug Geisler for their helpful comments in the manuscript. The authors would also like to thank the Max-Planck-Institut für Astronomie (MPIA Heidelberg) for hosting J.D. and P.M.F. during the completion of this work.

Funding for SDSS-III has been provided by the Alfred P. Sloan Foundation, the Participating Institutions, the National Science Foundation, and the U.S. Department of Energy Office of Science. The SDSS-III web site is <http://www.sdss3.org/>.

SDSS-III is managed by the Astrophysical Research Consortium for the Participating Institutions of the SDSS-III Collaboration including the University of Arizona, the Brazilian Participation Group, Brookhaven National Laboratory, Carnegie Mellon University, University of Florida, the French Participation Group, the German Participation Group, Harvard University, the Instituto de Astrofísica de Canarias, the Michigan State/Notre Dame/JINA Participation Group, Johns Hopkins University, Lawrence Berkeley National Laboratory, Max Planck Institute for Astrophysics, Max Planck Institute for Extraterrestrial Physics, New Mexico State University, New York University, Ohio State University, Pennsylvania State University, University of Portsmouth, Princeton University, the Spanish Participation Group, University of Tokyo, University of Utah, Vanderbilt University, University of Virginia, University of Washington, and Yale University.

Funding for the Sloan Digital Sky Survey IV has been provided by the Alfred P. Sloan Foundation, the U.S. Department of Energy Office of Science, and the Participating Institutions. SDSS-IV acknowledges support and resources from the Center for High-Performance Computing at the University of Utah. The SDSS web site is www.sdss.org.

SDSS-IV is managed by the Astrophysical Research Consortium for the Participating Institutions of the SDSS Collaboration including the Brazilian Participation Group, the Carnegie Institution for Science, Carnegie Mellon University, the Chilean Participation Group, the French Participation Group, Harvard-Smithsonian Center for Astrophysics, Instituto de Astrofísica de Canarias, The Johns Hopkins University, Kavli Institute for the Physics and Mathematics of the Universe (IPMU)/University of Tokyo, Lawrence Berkeley National Laboratory, Leibniz Institut für Astrophysik Potsdam (AIP), Max-Planck-Institut für Astronomie (MPIA Heidelberg), Max-Planck-Institut für Astrophysik (MPA Garching), Max-Planck-Institut für Extraterrestrische Physik (MPE), National Astronomical Observatories of China, New Mexico State University, New York University, University of Notre Dame, Observatório Nacional/MCTI, The Ohio State University, Pennsylvania State University, Shanghai Astronomical Observatory, United Kingdom Participation Group, Universidad Nacional Autónoma de México, University of Arizona, University of Colorado Boulder, University of Oxford, University of Portsmouth, University of Utah, University of Virginia, University of Washington, University of Wisconsin, Vanderbilt University, and Yale University.

This work has made use of data from the European Space Agency (ESA) mission *Gaia* (<https://www.cosmos.esa.int/gaia>), processed by the *Gaia* Data Processing and Analysis Consortium (DPAC, <https://www.cosmos.esa.int/web/gaia/dpac/consortium>). Funding for the DPAC has been provided by national institutions, in particular the institutions participating in the *Gaia* Multilateral Agreement.

This research made use of Astropy, a community-developed core Python package for Astronomy (Astropy Collaboration et al. 2018).

Facilities: Sloan (APOGEE), FLWO:2MASS, *Gaia*.

Software: Astropy.

ORCID iDs

Peter M. Frinchaboy  <https://orcid.org/0000-0002-0740-8346>

Julia O'Connell  <https://orcid.org/0000-0003-2321-950X>

Gail Zasowski  <https://orcid.org/0000-0001-6761-9359>

Ricardo Carrera  <https://orcid.org/0000-0001-6143-8151>

Kaike Pan  <https://orcid.org/0000-0002-2835-2556>

References

- Abolfathi, B., Aguado, D. S., Aguilar, G., et al. 2018, *ApJS*, 235, 42
- Bailer-Jones, C. A. L., Rybizki, J., Fouesneau, M., Mantelet, G., & Andrae, R. 2018, arXiv:1804.10121
- Basu, S., Grundahl, F., Stello, D., et al. 2011, *ApJL*, 729, L10
- Blanton, M. R., Bershad, M. A., Abolfathi, B., et al. 2017, *AJ*, 154, 28
- Bragaglia, A., Carretta, E., Gratton, R. G., et al. 2001, *AJ*, 121, 327
- Bragaglia, A., Sestito, P., Villanova, S., et al. 2008, *A&A*, 480, 79
- Bragaglia, A., Sneden, C., Carretta, E., et al. 2014, *ApJ*, 796, 68
- Bressan, A., Marigo, P., Girardi, L., et al. 2012, *MNRAS*, 427, 127
- Carraro, G., Ng, Y. K., & Portinari, L. 1998, *MNRAS*, 296, 1045
- Carraro, G., Villanova, S., Demarque, P., et al. 2006, *ApJ*, 643, 1151
- Carrera, R., & Pancino, E. 2011, *A&A*, 535, A30
- Carretta, E., Bragaglia, A., & Gratton, R. G. 2007, *A&A*, 473, 129
- Casamiquela, L., Carrera, R., Blanco-Cuaresma, S., et al. 2017, *MNRAS*, 470, 4363
- Cohen, J. G. 1980, *ApJ*, 241, 981
- Cunha, K., Frinchaboy, P. M., Souto, D., et al. 2016, *AN*, 337, 922
- Cunha, K., Smith, V. V., Johnson, J. A., et al. 2015, *ApJL*, 798, L41
- Cutri, R. M., Skrutskie, M. F., van Dyk, S., et al. 2003, The IRSA 2MASS All-Sky Point Source Catalog (Washington, D.C.: NASA)
- Dias, W. S., Alessi, B. S., Moitinho, A., & Lépine, J. R. D. 2002, *A&A*, 389, 871
- Donati, P., Bragaglia, A., Carretta, E., et al. 2015, *MNRAS*, 453, 4185
- Eisenstein, D. J., Weinberg, D. H., Agol, E., et al. 2011, *AJ*, 142, 72
- Friel, E. D. 1995, *ARA&A*, 33, 381
- Friel, E. D., Jacobson, H. R., & Pilachowski, C. A. 2010, *AJ*, 139, 1942
- Friel, E. D., & Janes, K. A. 1993, *A&A*, 267, 75
- Friel, E. D., Janes, K. A., Tavares, M., et al. 2002, *AJ*, 124, 2693
- Frinchaboy, P., Zasowski, G., Jackson, K., et al. 2010, JENAM 2010, Joint European and National Astronomy Meeting, 136
- Frinchaboy, P. M., & Majewski, S. R. 2008, *AJ*, 136, 118
- Frinchaboy, P. M., Thompson, B., Jackson, K. M., et al. 2013, *ApJL*, 777, L1
- Gaia Collaboration, Brown, A. G. A., Vallenari, A., et al. 2018, arXiv:1804.09365
- Gaia Collaboration, Prusti, T., de Bruijne, J. H. J., et al. 2016, *A&A*, 595, A1
- García Pérez, A. E., Allende Prieto, C., Holtzman, J. A., et al. 2016, *AJ*, 151, 144
- Geller, A. M., Mathieu, R. D., Braden, E. K., et al. 2010, *AJ*, 139, 1383
- Geller, A. M., Mathieu, R. D., Harris, H. C., & McClure, R. D. 2008, *AJ*, 135, 2264
- Gunn, J. E., Siegmund, W. A., Mannery, E. J., et al. 2006, *AJ*, 131, 2332
- Hole, K. T., Geller, A. M., Mathieu, R. D., et al. 2009, *AJ*, 138, 159
- Holtzman, J. A., Hasselquist, S., Shetrone, M., et al. 2018, *AJ*, 156, 125
- Holtzman, J. A., Shetrone, M., Johnson, J. A., et al. 2015, *AJ*, 150, 148
- Jacobson, H. R., Friel, E. D., & Pilachowski, C. A. 2009, *AJ*, 137, 4753
- Jacobson, H. R., Pilachowski, C. A., & Friel, E. D. 2011, *AJ*, 142, 59
- Janes, K. A. 1979, *ApJS*, 39, 135
- Jönsson, H., Allende Prieto, C., & Holtzman, J. A. 2018, *AJ*, 156, 126
- Kharchenko, N. V., Piskunov, A. E., Schilbach, E., Röser, S., & Scholz, R.-D. 2013, *A&A*, 558, A53
- Kubryk, M., Prantzos, N., & Athanassoula, E. 2015, *A&A*, 580, A127
- Lindgren, L., Hernandez, J., Bombrun, A., et al. 2018, arXiv:1804.09366
- Linden, S. T., Pryal, M., Hayes, C. R., et al. 2017, *ApJ*, 842, 49
- Magrini, L., Randich, S., Donati, P., et al. 2015, *A&A*, 580, A85
- Magrini, L., Randich, S., Kordopatis, G., et al. 2017, *A&A*, 603, A2
- Majewski, S. R., Schiavon, R. P., Frinchaboy, P. M., et al. 2017, *AJ*, 154, 94
- Majewski, S. R., Zasowski, G., & Nidever, D. L. 2011, *ApJ*, 739, 25
- Marigo, P., Giardi, L., Bressan, A., et al. 2008, *A&A*, 482, 883
- Mermilliod, J. C., Mayor, M., & Udry, S. 2008, *A&A*, 485, 303
- Minchev, I., Chiappini, C., & Martig, M. 2014, *A&A*, 572, A92
- Netopil, M., Paunzen, E., Heiter, U., & Soubiran, C. 2016, *A&A*, 585, A150
- Nidever, D. L., Holtzman, J. A., Allende Prieto, C., et al. 2015, *AJ*, 150, 173
- O'Connell, J. E., Frinchaboy, P. M., Shetrone, M., et al. 2018, *AJ*, submitted
- Origlia, L., Valenti, E., Rich, R. M., & Ferraro, F. R. 2006, *ApJ*, 646, 499
- Overbeek, J. C., Friel, E. D., & Jacobson, H. R. 2016, *ApJ*, 824, 75
- Pancino, E., Carrera, R., Rossetti, E., & Gallart, C. 2010, *A&A*, 511, A56
- Reddy, A. B. S., Giridhar, S., & Lambert, D. L. 2012, *MNRAS*, 419, 1350
- Reddy, A. B. S., Giridhar, S., & Lambert, D. L. 2013, *MNRAS*, 431, 3338
- Reddy, A. B. S., Giridhar, S., & Lambert, D. L. 2015, *MNRAS*, 450, 4301
- Reddy, A. B. S., Lambert, D. L., & Giridhar, S. 2016, *MNRAS*, 463, 4366
- Riello, M., de Angeli, F., Evans, D. W., et al. 2018, arXiv:1804.09367
- Schiappacasse-Ulloa, J., Tang, B., Fernández-Trincado, J. G., et al. 2018, *AJ*, 156, 94
- Sestito, P., Bragaglia, A., Randich, S., et al. 2008, *A&A*, 488, 943
- Smith, V. V., & Suntzeff, N. B. 1987, *AJ*, 93, 359
- Souto, D., Cunha, K., Smith, V., et al. 2016, *ApJ*, 830, 35
- Souto, D., Cunha, K., Smith, V. V., et al. 2018, arXiv:1803.04461
- Stassun, K. G., & Torres, G. 2018, arXiv:1805.03526
- Tautvaišienė, G., Edvardsson, B., Tuominen, I., & Ilyin, I. 2000, *A&A*, 360, 499
- The Astropy Collaboration, Price-Whelan, A. M., Sipőcz, B. M., et al. 2018, *AJ*, 156, 123
- Wilson, J. C., Hearty, F., Skrutskie, M. F., et al. 2012, *Proc. SPIE*, 8446, 84460H
- Wright, E. L., Eisenhardt, P. R. M., Mainzer, A. K., et al. 2010, *AJ*, 140, 1868
- Yong, D., Carney, B. W., & Friel, E. D. 2012, *AJ*, 144, 95
- Yong, D., Carney, B. W., & Teixeira de Almeida, M. L. 2005, *AJ*, 130, 597
- Zasowski, G., Cohen, R. E., Chojnowski, S. D., et al. 2017, *AJ*, 154, 198
- Zasowski, G., Johnson, J. A., Frinchaboy, P. M., et al. 2013, *AJ*, 146, 81